



## Increased late Pleistocene erosion rates during fluvial aggradation in the Garhwal Himalaya, northern India

Dirk Scherler <sup>a,b,c,\*</sup>, Bodo Bookhagen <sup>d,e</sup>, Hendrik Wulf <sup>f</sup>, Frank Preusser <sup>g</sup>, Manfred R. Strecker <sup>e</sup>

<sup>a</sup> Division of Geological and Planetary Sciences, California Institute of Technology, Pasadena, USA

<sup>b</sup> Earth Surface Geochemistry, Helmholtz Centre Potsdam GFZ German Research Centre for Geosciences, Potsdam, Germany

<sup>c</sup> Institute of Geological Sciences, Free University of Berlin, Berlin, Germany

<sup>d</sup> Department of Geography, University of California, Santa Barbara, USA

<sup>e</sup> Institute of Earth and Environmental Science, University Potsdam, Potsdam, Germany

<sup>f</sup> Department of Geography, University of Zurich, Zurich, Switzerland

<sup>g</sup> Institute of Earth and Environmental Sciences – Geology, University of Freiburg, Freiburg, Germany



### ARTICLE INFO

#### Article history:

Received 19 January 2015

Received in revised form 19 June 2015

Accepted 21 June 2015

Available online 29 July 2015

Editor: A. Yin

#### Keywords:

paleo-erosion rates

climate change

river terraces

landscape evolution

hillslopes

Himalaya

### ABSTRACT

The response of surface processes to climatic forcing is fundamental for understanding the impacts of climate change on landscape evolution. In the Himalaya, most large rivers feature prominent fill terraces that record an imbalance between sediment supply and transport capacity, presumably due to past fluctuations in monsoon precipitation and/or effects of glaciation at high elevation. Here, we present volume estimates, chronological constraints, and <sup>10</sup>Be-derived paleo-erosion rates from a prominent valley fill in the Yamuna catchment, Garhwal Himalaya, to elucidate the coupled response of rivers and hillslopes to Pleistocene climate change. Although precise age control is complicated due to methodological problems, the new data support formation of the valley fill during the late Pleistocene and its incision during the Holocene. We interpret this timing to indicate that changes in discharge and river-transport capacity were major controls. Compared to the present day, late Pleistocene hillslope erosion rates were higher by a factor of ~2–4, but appear to have decreased during valley aggradation. The higher late Pleistocene erosion rates are largely unrelated to glacial erosion and could be explained by enhanced sediment production on steep hillslopes due to increased periglacial activity that declined as temperatures increased. Alternatively, erosion rates that decrease during valley aggradation are also consistent with reduced landsliding from threshold hillslopes as a result of rising base levels. In that case, the similarity of paleo-erosion rates near the end of the aggradation period with modern erosion rates might imply that channels and hillslopes are not yet fully coupled everywhere and that present-day hillslope erosion rates may underrepresent long-term incision rates.

© 2015 Elsevier B.V. All rights reserved.

### 1. Introduction

Understanding the transient response of high-mountain landscapes to climate change is important for assessing the geomorphic impact of global warming and for unraveling potential linkages between climate, tectonics, and surface processes. For example, changes in temperature and precipitation can affect rates of weathering, runoff, and sediment transport (e.g., Tucker and Slingerland, 1997). How these changes combine and ultimately impact landscapes depends on their relative signs and magnitudes. River

terraces are arguably the most common landforms used to infer climate change impacts on landscapes, because they record periods of valley aggradation and incision that are typically related to changes in runoff and sediment supply (e.g., Bull, 1991). Whereas changes in runoff can, at least qualitatively, be inferred from paleoclimatic records, changes in hillslope sediment supply are more difficult to assess and often remain speculative.

In the past two decades, significant advances in understanding and quantifying hillslope weathering and erosion have been achieved with *in situ*-produced terrestrial cosmogenic nuclides (TCN), which are rare isotopes that are produced by cosmic radiation in the uppermost meters of the Earth's surface (e.g., Lal, 1991). In particular, catchment-average erosion rates, derived from TCN abundances in river sediments, have propelled new insights into relations between erosion, climate, tectonics,

\* Corresponding author at: Earth Surface Geochemistry, Helmholtz Centre Potsdam GFZ German Research Centre for Geosciences, Potsdam, Germany. Tel.: +49 331 288 28646.

E-mail address: scherler@gfz-potsdam.de (D. Scherler).

and topography (e.g., Granger et al., 1996; Riebe et al., 2001; Scherler et al., 2014a). TCNs in fluvial sediments integrate hillslope erosion rates over time spans that are roughly equal to the time it takes for eroding the uppermost 60–100 cm, that is,  $\sim 10^2\text{--}10^4$  yr in most tectonically active landscapes. Such time scales are usually long enough to avoid anthropogenic land use changes, but short enough to potentially detect climate-induced erosion rate changes (von Blanckenburg, 2005).

A promising application for studying landscape response to climate change is measuring TCN abundances in ancient fluvial deposits to obtain paleo-erosion rates for entire catchments (Schaller et al., 2002; Charreau et al., 2011; Bekaddour et al., 2014). However, this approach has not been often used and its applicability in different landscapes remains to be tested (Schaller and Ehlers, 2006). Here, we study hillslope erosion rates during a late Quaternary episode of river aggradation in the Garhwal Himalaya, northern India, by comparing TCN concentrations in recent and ancient fluvial sediments. We supplement these data with chronological constraints on the aggradation period and an assessment of the amount of transiently stored material to test existing models of geomorphic response to climate change in the Himalaya.

## 2. Geomorphic response to climate change in the Himalaya

Throughout the Himalaya, remnants of thick valley fills straddle most major transverse drainages and testify to periods of transient imbalances between hillslope sediment supply and river capacity. Although some of these fills are clearly due to landslide dams (e.g., Bookhagen et al., 2005; Pratt-Sitaula et al., 2007) or glacier dams (e.g., Scherler et al., 2014b), many others have been linked to climate change (e.g., Lavé and Avouac, 2001). In the Marsyandi Valley, Nepal (Pratt et al., 2002) and the Sutlej Valley, India (Bookhagen et al., 2006), the most recent period of aggradation has been related to a pulse of enhanced sediment supply that overwhelmed river capacity during a phase of intensified monsoon precipitation in the early Holocene (Fig. 1a). Enhanced precipitation is assumed to have resulted in higher pore pressures on hillslopes that would have triggered landslides more frequently (Carson, 1976; Pratt et al., 2002); hence we refer to this model as ‘hillslope-driven aggradation’. An alternative model, which is mainly based on comparison of fluvial chronologies from the Alaknanda River, NW India, with paleoclimatic records, has related aggradation to reduced river discharge during a phase of weakened monsoon precipitation in the late Pleistocene and ensuing incision to a phase of strong monsoon precipitation (Srivastava et al., 2008; Juyal et al., 2010; Ray and Srivastava, 2010). Because changes in hillslope sediment flux are of minor importance relative to changes in river discharge and transport capacity, we term this model ‘discharge-driven aggradation’ (Fig. 1b).

The main testable differences between these two models are (1) the timing and rate of aggradation and (2) the coupling between hillslopes and rivers. Depositional ages are currently only available from the Alaknanda Valley and support the discharge-driven model, but significant differences in between studies (Srivastava et al., 2008; Ray and Srivastava, 2010; Juyal et al., 2010) complicate a clear correlation with climatic variations. If aggradation occurred during the late Pleistocene in the Sutlej and Marsyandi Valleys, too, it does not preclude the possibility that it was driven by enhanced hillslope sediment supply during earlier humid periods. Moreover, modeling work suggest that hillslope-driven aggradation can also occur due to changes in vegetation cover or runoff intensity without changing mean annual precipitation (Tucker and Slingerland, 1997). Therefore, the temporal correlation of landforms with climatic records may not be enough to distinguish between these models.

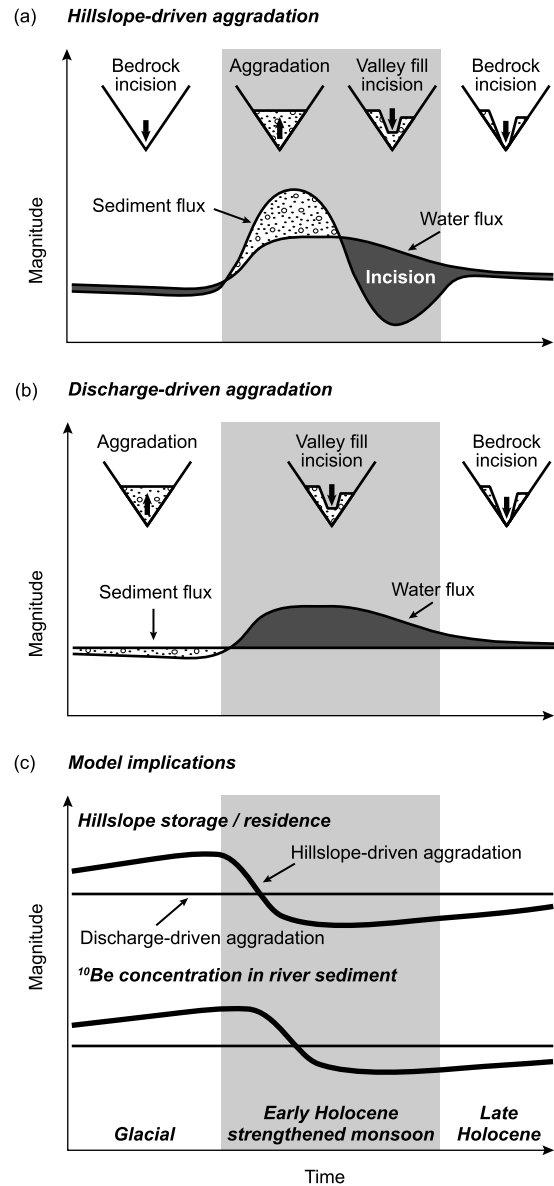


**Fig. 1.** Sketch showing different models of river response to climate change in the Himalaya. (a) Hillslope-driven aggradation (modified after Pratt et al., 2002). (b) Discharge-driven aggradation. (c) Model implications for hillslope storage and  $^{10}\text{Be}$  concentrations in river sediment. Note that  $^{10}\text{Be}$  concentrations in river sediments are damped and lag behind hillslope storage due to finite integration times (e.g., Schaller and Ehlers, 2006).

Changes in hillslope erosion rates due to changes in weathering and soil production, for example, could principally occur in both models. However, it is central to the hillslope-driven model that during a period of reduced landsliding, hillslopes temporarily accumulate weathered material that is later removed during a period of enhanced landsliding and other mass movements (Pratt et al., 2002; Bookhagen et al., 2005). Such temporal variations in hill-slope sediment storage and residence time reflect changes in hillslope erosion rates and thus the accumulation of TCNs (Fig. 1c). In the hillslope-driven model, TCN concentrations (erosion rates) are expected to decrease (increase) during aggradation as the ‘hillslope reservoir’ is progressively depleted. In addition to chronologic data, comparison of TCN abundances in fluvial sediments from rivers and terraces should therefore help distinguishing between hillslope-driven and discharge-driven aggradation. We will test this approach in the Garhwal Himalaya of Northern India.

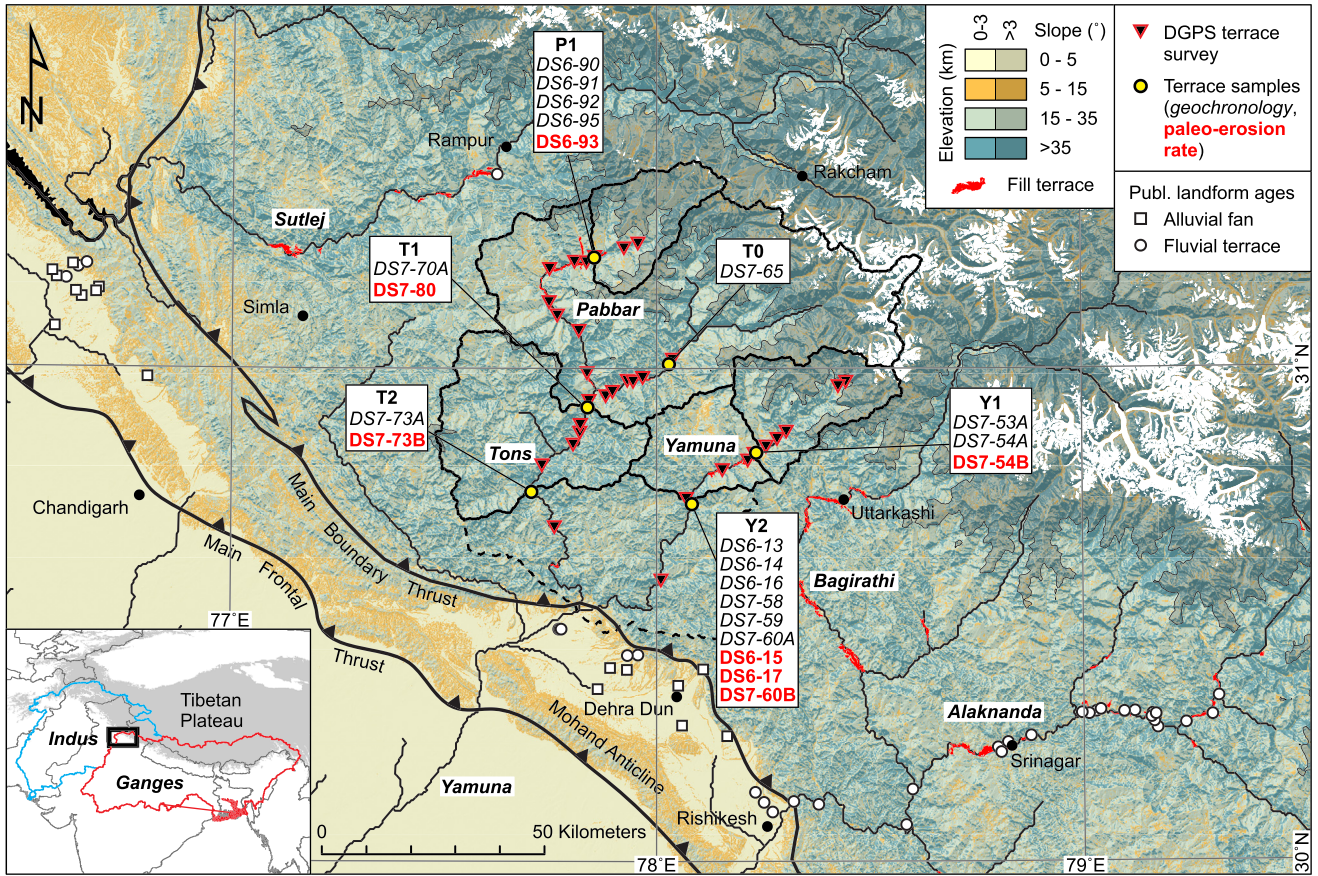


**Fig. 2.** Overview of the study area in the Yamuna catchment, Garhwal Himalaya, NW India. Slope-map draped over hillshade map with elevations >3 km darker. White areas show present-day ice cover (Arendt et al., 2012), red areas indicate fill terraces. Major rivers are shown in bold italics. Yellow circles give sample locations, white squares and circles denote published landform ages (Singh et al., 2001; Bookhagen et al., 2005; Suresh et al., 2007; Srivastava et al., 2008; Sinha et al., 2010; Ray and Srivastava, 2010; Dutta et al., 2012), and black points are towns. (For interpretation of the references to color in this figure legend, the reader is referred to the web version of this article.)



**Fig. 3.** Field photograph of fill terraces in the Yamuna Valley, at location Y2 (see Fig. 2). Sample locations are marked by a white 'x'. View downstream along the Yamuna River, which is seen in the lower left corner. Terrace deposits are exposed by road cut in tributary valley. Note that pronounced lithological contrasts between Yamuna and tributary gravels ensure the distinction of provenance in outcrops.

### 3. Study area and previous work

The Garhwal Himalaya hosts the westernmost headwaters of the Ganges drainage system that discharges into the Bay of Bengal (Fig. 2). Our study area comprises the Yamuna catchment in the

western Garhwal Himalaya, which is drained by three main rivers: the Yamuna and Tons rivers, and the Pabbar River, which is a tributary of the Tons. The lower part of the Yamuna catchment, with elevations below ~3000 m, is referred to as the Lesser Himalaya and is dominated by metasedimentary rocks of the Lesser Himalayan Sequence (LHS) that are overlain by higher-grade metamorphic LHS rocks. At elevations above 3000 m, high-grade metamorphic and intrusive rocks of the High Himalayan Sequence (HHS) dominate the High Himalaya (Gansser, 1964). Along all major rivers in the Yamuna catchment and far upstream of presently active faults exist remnants of a thick fluvial valley fill, with prominent and generally well-preserved terrace surfaces (Fig. 3). It is important to note that the confluence of the Yamuna and Tons rivers is located in the Dehra Dun basin, which is a piggy-back basin between the Main Boundary Thrust (MBT) in the north, and the Mohand Anticline atop the Main Frontal Thrust (MFT) in the south (Fig. 2), and that deposition in one valley therefore cannot have caused simple back-filling in the other.

At present, the majority of precipitation falls between June and September, when the southwest Indian monsoon impinges on the southern front of the Himalaya. During winter and spring so-called western disturbances occasionally pass through the area and cause snowfall down to elevations of ~1000 m (Scherler et al., 2014a). Total annual rainfall reaches >1500 mm yr<sup>-1</sup> in much of the study area with peaks of up to ~4000 mm yr<sup>-1</sup> (Bookhagen and Burbank, 2010). Currently no studies exist that constrain the late Quaternary monsoon history in the study area, but most marine and terrestrial records from the greater South Asian region show that the Indian monsoon intensity has strongly varied along with

changes in solar insolation (e.g., Clemens et al., 1991). The termination of the last glacial period was characterized by the transition from a cooler and relatively more arid climate to a warmer and more humid climate in the early Holocene, followed by gradual cooling and less humid conditions from the mid- to late Holocene (Herzschuh, 2006). In the upper Tons Valley, this climatic transition forced a slow and stepped recession of glaciers throughout the Holocene, with the largest glaciers reaching down to ~2500 m at ~16 ka (Scherler et al., 2010). In the Yamuna and Pabbar valleys, however, valley morphologies and Quaternary deposits indicate no significant glacial overprints.

In a previous study, Scherler et al. (2014a) determined catchment-averaged erosion rates from  $^{10}\text{Be}$  concentrations in modern river sediment, collected from active channels of 18 tributaries throughout the study area and at six locations along the Yamuna, Tons, and Pabbar rivers. The magnitude of tributary erosion rates largely reflects the topographic steepness (e.g., local relief, channel steepness) and is generally close to expected rock uplift rates that would result from rigid sliding of the orogenic wedge over the ramp-flat geometry of the Main Himalayan Thrust fault, suggesting near-steady state topography in the tributaries (Scherler et al., 2014a). However, there exist discrepancies of up to ~60% between main stem-erosion rates derived from  $^{10}\text{Be}$  and from calibrated functional relationships between hydro-morphological parameters and the tributary erosion rates. This could be related to insufficient mixing of sediments within the trunk rivers and thus methodological problems, as has been suggested for other large Himalayan watersheds (Lupker et al., 2012). Alternatively, the functional relationships could simply not capture all controls on erosion. In any case, such additional uncertainties should be kept in mind and limit the potential to detect temporal variations in erosion rates when comparing samples from main stem rivers in the Himalaya.

#### 4. Data and methods

##### 4.1. Field mapping and topographic analyses

Fluvial fill terraces were mapped on the basis of 1:100,000 topographic maps, ASTER and SPOT satellite images at finer spatial scales, and using a handheld GPS. More detailed surveys of individual terrace surfaces were conducted with a differential GPS (Trimble 5700/5800) in post-processing kinematic mode with sub-meter accuracy. Along any given reach, we focused on surveying the spatially most extensive and well-preserved topmost terrace surfaces. We supplemented our field surveys with topographical analyses of a 90-m resolution SRTM digital elevation model (DEM). Drainage networks and catchment boundaries were extracted using MATLAB® and the TopoToolbox v2 (Schwanghart and Scherler, 2014).

##### 4.2. Dating

To constrain the fluvial aggradation history and obtain numerical ages of the mapped fill terraces, we collected a total number of 14 samples for  $^{14}\text{C}$  and luminescence dating, and two samples for TCN surface exposure dating (Table 1). Whereas the  $^{14}\text{C}$  and luminescence ages stem from terrace sediments and provide depositional ages during river aggradation, the TCN exposure ages from terrace surfaces provide an estimate of the onset of incision.  $^{14}\text{C}$  in charcoal fragments were analyzed by accelerator mass spectrometry (AMS) at the Leibniz-Laboratory for Radiometric Dating and Isotope Research in Kiel, Germany. All of the  $^{14}\text{C}$  samples have  $\delta^{13}\text{C}$  values within the range of standard values and are considered reliable (Table EA1). Conventional  $^{14}\text{C}$  ages were calibrated using CALIB 7.0 (Reimer et al., 2013).

**Table 1**  
Geochronology sample results.

Sample name	Locality	Material	Latitude (°N)	Longitude (°E)	Sample elevation (m)	River elevation (m)	Elevation of valley fill (m)	Estimated bedrock elevation (m)	Dating method	Calendar age (ka BP) <sup>a</sup>
Tons River										
D57-65	T0	Pebbles	31.0169	78.0372	1194	1145	1194	1080	$^{10}\text{Be}$	$9.81 \pm 0.86$
D57-70A	T1	Sand	30.9206	77.8371	954	890	960	840	OSL	$13.48 \pm 0.81$
D57-73A	T2	Sand	30.7496	77.7055	845	740	870	735	OSL	$10.75 \pm 0.57$
Yamuna River										
D56-13	Y2	Charcoal dust	30.7408	78.0767	990	965	1095	850	$^{14}\text{C}$	$23.96 \pm 0.58$
D56-14	Y2	Charcoal pieces	30.7408	78.0767	1000	965	1095	850	$^{14}\text{C}$	$47.06 \pm 3.46$
D56-16	Y2	Sand	30.7408	78.0767	1000	965	1095	850	OSL	$13.10 \pm 2.30$
D56-16	Y2	Sand	30.7408	78.0767	1000	965	1095	850	IRSL	$41.70 \pm 3.10$
D57-58	Y2	Sand	30.7362	78.0668	1179	965	1095	850	OSL	$31.30 \pm 1.90$
D57-60A	Y2	Sand	30.7248	78.0814	999	955	1080	840	OSL	$9.70 \pm 1.00$
D57-53A	Y1	Sand	30.8231	78.2284	1283	1200	1290	1125	OSL	$13.00 \pm 1.00$
D57-54A	Y1	Sand	30.8218	78.2293	1249	1200	1290	1125	OSL	$23.60 \pm 1.60$
Pabbar River										
D56-90	P1	Charcoal pieces	31.2144	77.8363	1692	1640	1700	1595	$^{14}\text{C}$	$26.23 \pm 1.65$
D59-91	P1	Charcoal pieces	31.2250	77.8326	1678	1675	1730	1615	$^{14}\text{C}$	$0.51 \pm 0.04$
D56-92	P1	Sand	31.2250	77.8327	1679	1675	1730	1615	OSL	$14.20 \pm 3.70$
D56-92	P1	Sand	31.2250	77.8327	1679	1675	1730	1615	IRSL	$36.70 \pm 2.80$
D56-95	P1	Sand	31.2142	77.8334	1690	1640	1697	1590	OSL	$12.70 \pm 4.50$
D56-95	P1	Sand	31.2142	77.8334	1690	1640	1697	1590	IRSL	$31.50 \pm 2.80$

<sup>a</sup> Calibrated  $^{14}\text{C}$  ages based on CALIB 7.0 (Reimer et al., 2013);  $^{10}\text{Be}$ -surface exposure ages based on production rate scaling scheme by Lal (1991), as updated by Stone (2000) and implemented by Balco et al. (2008) in the CRONUS online calculator. See text for details.

Quartz grains from six samples (Table EA2) were dated using optically stimulated luminescence (OSL) at the Sheffield Centre for International Drylands Research, UK, following standard sample preparation procedures and using the single aliquot regenerative dose protocol (Murray and Wintle, 2000). In the case of a broad distribution of single-aliquot values (overdispersion >20%), finite-mixture modeling was applied to isolate the dominant peak. Three more samples (Table EA2) were analyzed by similar procedures at the University of Bern, Switzerland, where additionally infrared stimulated luminescence (IRSL) dating of K-feldspar grains was carried out (see supplemental information for details). For further discussion, it is important to note that the quartz OSL signal shows a strong medium component, which can lead to underestimation of ages (Steffen et al., 2009b). On the other hand, K-feldspar IRSL is also problematic, in particular with regard to signal stability, and tends to underestimate the real deposition age. While recent methodological progress is overcoming this problem, the samples presented here were analyzed in 2008 and the feldspar fraction of the Sheffield samples was not retained. As a consequence, the results of the OSL and IRSL dating have to be considered with caution.

TCN exposure dating was done on one sample of amalgamated gravels (~5 cm diameter,  $n > 30$ ) from a terrace surface in the Yamuna Valley (DS7-59) and on one sample of amalgamated rock chips from 12 meter-sized boulders on a terrace surface in the Tons Valley (DS7-65; Fig. 2; Table EA3). The exposure ages were calculated using the CRONUS v2.2 online calculator (Balco et al., 2008). More details on the analytical sample results and the dating procedures are provided in the supplementary data (Figs. S1–S4) and the electronic appendix (Tables EA1–EA3).

#### 4.3. $^{10}\text{Be}$ -derived paleo-erosion rates

We collected seven samples from fluvial fill terraces at five locations along the Yamuna (Y1, Y2), Tons (T1, T2), and Pabbar (P1) trunk rivers (Table 2) that are close to previous sample locations of the modern channel (Scherler et al., 2014a), to ensure identical upstream areas (Fig. 2). To minimize TCN production after burial and incision of the valley fill, we collected the terrace samples at road-cut outcrops, which were >10 m below any terrace surface and where the samples had been laterally shielded by at least ~4–5 m of material prior to exposure (Fig. 3). To allow for direct comparison of our terrace samples with the samples from the active channels, we applied the same analytical procedures as in Scherler et al. (2014a): We separated the 125–500  $\mu\text{m}$  sized quartz fraction by standard physical and chemical methods, including magnetic and heavy-liquid separation, and removal of non-quartz minerals in heated hydrochloric and hydrofluoric acid baths. After adding ~200  $\mu\text{g}$   $^{9}\text{Be}$  as spike, the samples were dissolved in concentrated hydrofluoric acid and Beryllium was extracted by ion-exchange chromatography. Accelerator mass spectroscopy (AMS) measurements were done at Lawrence Livermore National Laboratories, USA. The subtracted process blank has a  $^{10}\text{Be}/^{9}\text{Be}$  ratio of  $3.9 \times 10^{-15}$ .

Determining erosion rates from TCN concentrations requires site-specific production rates, which are known to vary temporally due to changes in the geomagnetic field and atmospheric density, but can also vary due to changes in surface coverage. While the employed time-dependent production rate scaling model ('Lm' in Balco et al., 2008) attempts to account for geomagnetic field effects (results from other production rate scaling models are shown in Table EA4), changes in atmospheric density in the study area are probably <5% (Staiger et al., 2007). Changes in ice cover, snow, and vegetation are more difficult to constrain and merit special attention. Because of poor constraints, we did not attempt to adjust production rates due to changes in ice and vegetation cover during

**Table 2**  
 $^{10}\text{Be}$  terrace sample data.

Sample ID	Locality	Lat (°N)	Lon (°E)	Sample elevation (m)	Up- stream area (km <sup>2</sup> )	Mean catchment elevation (m)	Catchment glacial cover (%)	$^{10}\text{Be}$ concentration ( $10^3$ at g <sup>-1</sup> )	Shielding factors		
									Topography	Ice cover	Snow cover ( $\Delta\text{SL} = 500$ m) <sup>a</sup>
DS6-93	P1	31.2262	77.8519	1679	516	3314	0.2	16.83 ± 0.45	0.96	1.00	0.92
DS7-80	T1	30.9185	77.893	941	3478	3015	3.6	8.30 ± 0.32	0.95	0.96	0.92
DS7-73C	T2	30.7495	77.7048	845	4678	2747	2.7	23.29 ± 0.61	0.96	0.97	0.94
DS7-54B	Y1	30.8209	78.2281	1249	647	2976	1.0	13.04 ± 0.36	0.95	0.99	0.93
DS6-17	Y2	30.7381	78.0793	1030	1150	2493	0.5	13.81 ± 0.48	0.96	0.99	0.96
DS6-15	Y2	30.7380	78.0791	1000	1150	2493	0.5	9.77 ± 0.27	0.96	0.99	0.96
DS7-60B	Y2	30.7244	78.0805	999	1179	2474	0.5	24.63 ± 0.64	0.96	0.99	0.96

<sup>a</sup>  $\Delta\text{SL}$  = snowline lowering.

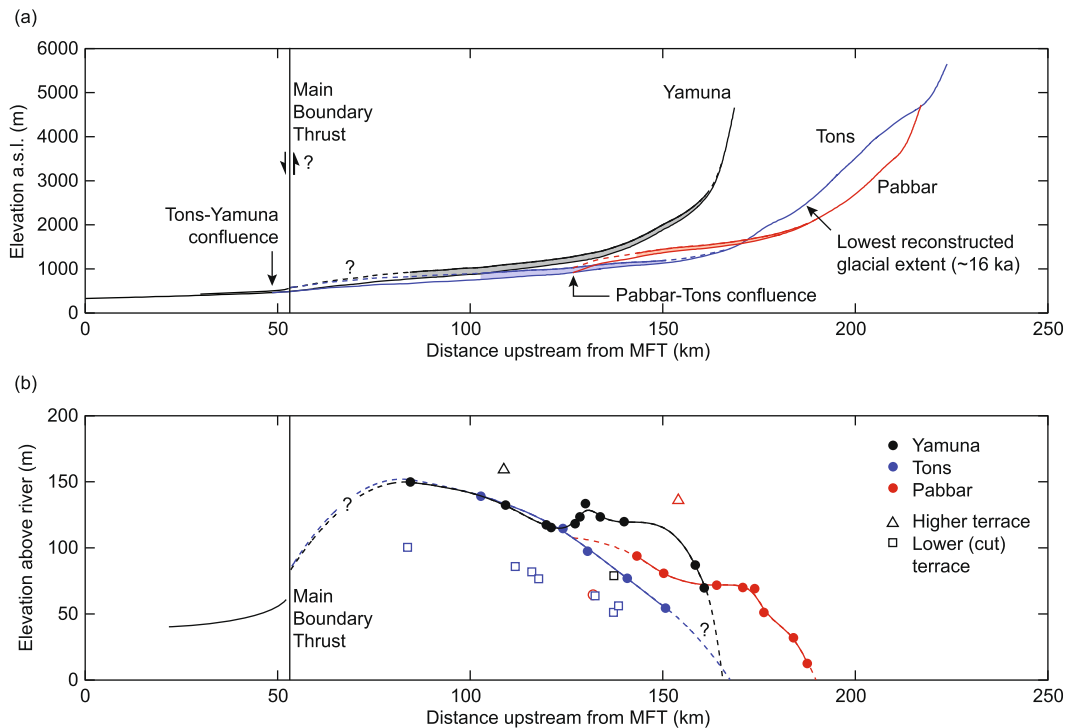


**Fig. 4.** Distribution of valley fills along the main rivers in the Yamuna catchment. (a) Elevation of river long profiles and top valley fill surfaces. (b) Differential GPS-surveyed terrace elevations above the active channel. Each data point comprises the average of all DGPS-derived surface elevations from an individual terrace surface, projected into a vertical plane that follows the river channel. MFT = Main Frontal Thrust.

the time of aggradation, but we will address these issues in the discussion of our results.

We accounted for snow-cover shielding with a simple phenomenological approach that is based on present-day durations of snow-coverage derived from remote sensing observations that we converted to snow depths by comparison with available snow depth-time series (see Scherler et al., 2014a, for details). For the sample locations considered in this study, the maximum correction of production rates due to present-day snow cover shielding is 8% (Table 2). In order to assess the potential impact of increased snow coverage in the past, we artificially lowered the remote-sensing based climatic snowline by 500 m and 1000 m, which resulted in longer snow-cover durations throughout the study area, and employed the same relationship between snow depth and snow cover duration as for the present-day samples.

## 5. Results

### 5.1. Valley fill geometry

The topmost elevation of the valley fill ranges between ~750 and ~1180 m along the Tons River, between ~930 and ~2600 m along the Yamuna River, and from its confluence with the Tons at ~930 m to an elevation of ~2030 m along the Pabbar River (Fig. 4a). At their lowest occurrence in the Tons and Yamuna valleys these surfaces are located at almost 150 m above the present-day river. Their height above the river decreases upstream, first rather gradually but towards the headwater areas more rapidly (Fig. 4b). In the Tons Valley, downstream of the Tons-Pabbar confluence, a prominent terrace level is cut at ~2/3 of the topmost section of the valley fill (Fig. 4b). Several other cut terraces that we did not survey, are sculpted at different heights into the valley fill (Fig. 3). Because we did not find well-preserved terrace surfaces in the lower parts of the Tons and Yamuna valleys that could be clearly linked with the terrace surfaces farther upstream, the downstream continuation of the valley fill is more difficult to con-

strain. We also found fluvial deposits located above the topmost surface of the valley fill, but most of these do not have well-preserved terrace surfaces. We surveyed two of the higher surfaces in the Yamuna and Pabbar valleys at 110 km and 155 km distance north of the MFT, respectively (Fig. 4b). Among the highest gravel-bearing surfaces are fluvial-terrace deposits at ~95 km distance from the MFT in the Tons Valley, ~260 m above the present-day river, and at ~110 km distance from the MFT in the Yamuna Valley, ~250 m above the present-day river. We interpret these deposits to be related to older valley-filling periods, which we did not consider any further in this study.

To estimate the total volume of the prominent valley fill in the trunk valleys, we interpolated the topmost surfaces, and extrapolated them along the entire length of the three rivers by assuming a gradual decline upstream and a more steeply, parabolic decline downstream that approximately results in continuity with terrace surfaces found at the Tons-Yamuna confluence, near the MBT (Fig. 4b). We acknowledge ambiguity in our reconstruction in the lower part of the Tons and Yamuna valleys, but as most of the late Pleistocene shortening in this region of the Himalaya is thought to be accommodated along the MFT (Powers et al., 1998), it is reasonable to assume no large (>50 m) offsets between terrace surfaces on either side of the MBT.

With the interpolated elevation of the valley fill and by assuming a cross-valley constant elevation, we reconstructed the former valley bottom at the end of the aggradation period. The calculated volume between the present-day topography and the former valley bottom equals 10.2 km<sup>3</sup>. Because bedrock has not yet been reached everywhere, this number is likely a lower estimate of the total volume. By projecting the hillslopes above the valley fill with an average angle of 25° (Fig. S6) into the subsurface, we estimated the volume of the valley fill that is still stored in the trunk valleys to be ~3.6 km<sup>3</sup>, resulting in a total volume of ~13.8 km<sup>3</sup>, with 2.3, 5.3, and 6.2 km<sup>3</sup> stored in the Pabbar, Tons, and Yamuna valleys, respectively (Fig. S7). Distributed across the hillslopes, and adjusted for density differences

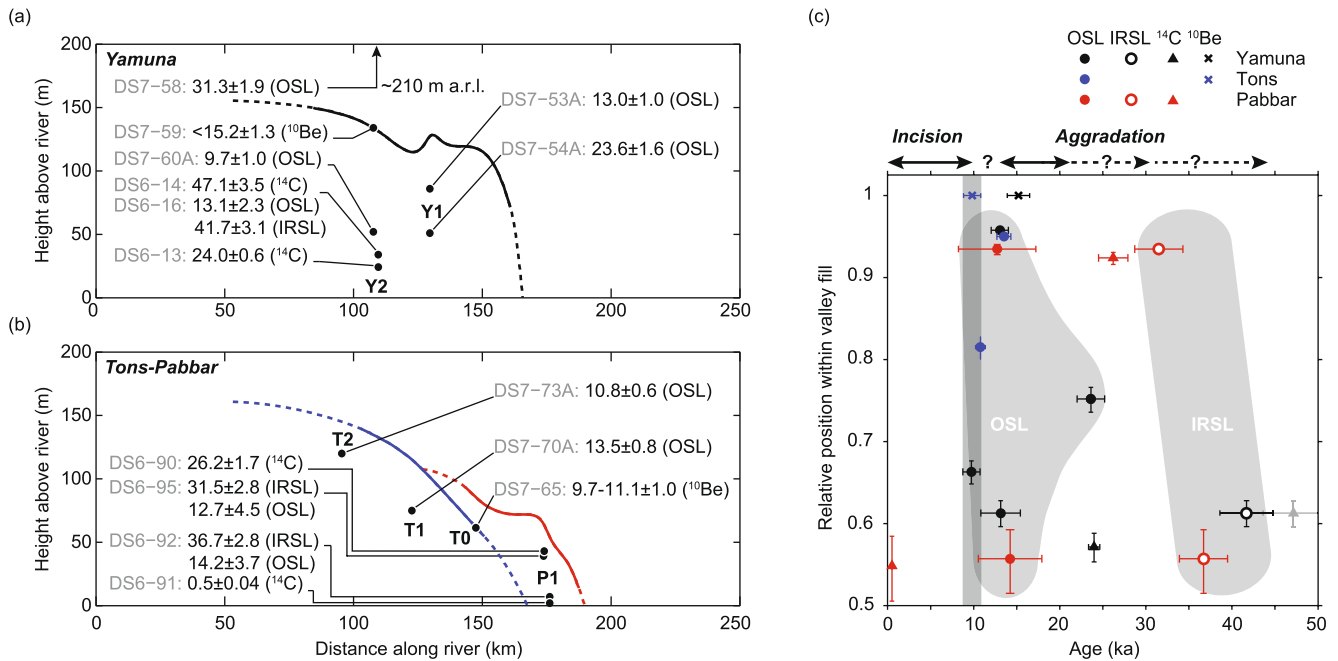


**Fig. 5.** Terrace chronological data along (a) the Yamuna River, and (b) the Tons and Pabbar rivers. All ages in ka with  $2\sigma$  uncertainties. All samples are derived from the main valley fill, except DS6-091, which is from an inset fill near the present-day river. (c) Terrace ages with respect to their relative position within the valley fill. Light-gray areas encircle depositional ages obtained by different dating methods. Vertical dark-grey bar denotes  $^{10}\text{Be}$ -derived minimum surface exposure age indicating latest possible onset of incision.  $^{14}\text{C}$  age >45 ka (faint symbol) is likely from reworked material. Y-axis error bar is based on  $\pm 10$  m uncertainty in estimated bedrock elevation.

( $\rho_{\text{bedrock}} = 2.7 \text{ g cm}^{-3}$ ;  $\rho_{\text{sediment}} = 1.7 \text{ g cm}^{-3}$ ), these volumes are equal to 1.0, 0.9, and 1.8 m of bedrock thickness in the Pabbar, Tons, and Yamuna valleys, respectively. With an average erosion rate of  $\sim 0.7 \text{ mm yr}^{-1}$  for the entire Yamuna catchment (Lupker et al., 2012; Scherler et al., 2014a), and assuming that the entire valley fill is related to one aggradation phase, it would have taken only  $\sim 1.3$ – $2.6$  kyr to erode this volume of rock. Acknowledging that the terrace deposits constitute mostly bedload, which may represent only 10–50% of the total load (Pratt-Sitaula et al., 2007; Wulf et al., 2010), this duration could increase to 2.6– $26.3$  kyr, and even longer, if the bedload trapping efficiency was less than 100%. Clearly, additional constraints on the timing and duration of aggradation are needed.

## 5.2. Terrace chronology

Well-rounded crystalline gravels and cobbles of the LHS and HHS dominate the examined valley fill deposits (Figs. S8–S47). At most of the studied outcrops, bedding is only weakly expressed and best seen by occasional sand lenses of decimeter-scale thickness and meter-scale length, from which we collected our luminescence samples. At confluences with tributaries that drain a distinctly different lithology (e.g., metasedimentary rocks of the LHS), intercalation of main stem with tributary deposits can be seen. The tributary deposits often display more angular grains, a higher amount of fine matrix and poor sorting, similar to debris-flow deposits. Charcoal pieces for  $^{14}\text{C}$  dating were collected from fine-grained layers deposited in backwater ponds of small extent as well as from more massive deposits.

In the Yamuna Valley, we collected seven terrace sediment samples at two different locations (Fig. 2; Table 1). At the lower site, three of our samples (DS6-13, -14, -16) were taken from below a younger cut terrace (Fig. 3), but lateral continuity of the sampled material beneath the terrace riser ascertains its deposition during the same aggradation phase. Although we did not observe any discontinuities in the stratigraphy of the sampled deposits (Fig. 3), such as paleosols or erosive contacts, the ages we ob-

tained from  $^{14}\text{C}$ , OSL, and IRSL, are conflicting (Fig. 5a). First, the stratigraphically higher  $^{14}\text{C}$ -sample (DS6-14) yielded an older calibrated age,  $47.1 \pm 3.5$  ka, compared to the stratigraphically lower  $^{14}\text{C}$ -sample (DS6-13), with a calibrated age of  $24.0 \pm 0.6$  ka. Second, a sand sample (DS6-16) taken at the same location as DS6-14 yielded strikingly different ages from OSL ( $13.1 \pm 2.3$  ka) and IRSL ( $41.7 \pm 3.1$  ka), which are both lower than the  $^{14}\text{C}$  age. Two kilometers farther downstream, a sample from a stratigraphically higher elevation yielded an OSL age of  $9.7 \pm 1.0$  ka. A sample from deposits  $\sim 200$  m above the present-day channel, which presumably stems from an older valley fill/aggradation period, yielded an OSL age of  $31.3 \pm 3.0$  ka. 20 km farther upstream the Yamuna River, we obtained OSL ages of  $23.6 \pm 1.6$  ka (DS7-54A) and  $13.0 \pm 1.0$  ka (DS7-53A), in correct stratigraphic order.

In the Tons Valley,  $\sim 30$  km apart, at similar depth below the valley fill surface (Fig. 5b), two OSL ages of  $10.8 \pm 0.6$  ka (DS7-73A) and  $13.5 \pm 0.8$  ka (DS7-70A) are available. In the Pabbar Valley, one sample from the base of the valley fill near the present-day channel (DS6-92) yielded an OSL age of  $14.2 \pm 3.7$  ka and an IRSL age of  $36.7 \pm 2.8$  ka. Another  $^{14}\text{C}$ -sample is from a small inset fill that, perched against the larger valley fill, protrudes  $\sim 5$  m above the present-day channel (DS6-91) and yielded a calibrated age of  $0.5 \pm 0.04$  ka. Two kilometers downstream, at the confluence with a tributary, a sample from near the top of the valley fill (DS6-95) yielded an OSL age of  $12.7 \pm 4.5$  ka and an IRSL age of  $31.5 \pm 2.8$  ka, whereas the other, stratigraphically slightly higher  $^{14}\text{C}$  sample yielded a calibrated age of  $26.2 \pm 1.7$  ka.

Finally, the amalgamated cobble sample from a terrace surface in the Yamuna Valley (DS7-59), yielded a  $^{10}\text{Be}$ -surface exposure age of  $13.6 \pm 1.2$  ka assuming no mixing of the soil, which however is unlikely due to active farming on the surface. If we assume the topmost 30 cm are thoroughly mixed and use an average production rate corresponding to  $\sim 15$  cm depth, the exposure age increases to  $\sim 15.2 \pm 1.3$  ka. Because we have no constraints on the inherited  $^{10}\text{Be}$  concentration, we consider this to be a maximum age. The inherited component of our amalgamated rock-chips sample from a terrace surface in the Tons Valley, which yielded a

$^{10}\text{Be}$ -surface exposure age of  $9.8 \pm 0.9$  ka, is likely much smaller than for the cobble sample, but it is also likely that the sampled surfaces have experienced some erosion. We therefore consider this to be a minimum age.

### 5.3. $^{10}\text{Be}$ -derived paleo-erosion rates

The measured  $^{10}\text{Be}$  concentrations are shown in Table 2. Because production rates vary with time, the derived paleo-erosion rates depend on the depositional ages, which are, unfortunately, not well constrained. To elucidate the effect of temporally changing production rates, we calculated paleo-erosion rates for three different depositional ages (10, 20, and 40 ka), which approximately span the range of terrace ages we obtained (Fig. 5). As temporal changes in production rates are substantial in our study area, paleo-erosion rates differ by up to 30% for depositional ages of 10 and 40 ka and range from  $\sim 0.6\text{--}2.2 \text{ mm yr}^{-1}$  for a depositional age of 10 ka, to  $\sim 0.8\text{--}2.9 \text{ mm yr}^{-1}$  for a depositional age of 40 ka (Table 3). If snowline elevations had been 500 m lower during the accumulation of  $^{10}\text{Be}$  in our terrace samples, the erosion rates would have been lower by on average ( $\pm 1\sigma$ )  $6.2 \pm 2.2\%$ , and by  $12.0 \pm 2.8\%$  for a snowline lowering of 1000 m (assuming a depositional age of 20 ka).

## 6. Discussion

### 6.1. Timing of aggradation and incision

Establishing a reliable depositional chronology for the investigated sediments is complicated by the poor properties of the quartz OSL signal (Fig. S1). It has been shown that the absence of a dominant fast OSL signal component can lead to underestimation of quartz OSL ages (Steffen et al., 2009b). Indeed, the feldspar ages are two to three times greater than the quartz ages in the three samples where both fractions were dated. As the feldspar samples have narrow dose distributions (Fig. S4), explaining this offset by incomplete bleaching of IRSL appears unlikely. Based on previous experience with similar problems (Steffen et al., 2009a, 2009b), we suspect that the quartz ages are underestimating the real age of deposition and hence provide us only with minimum ages. As no storage tests have been carried out to monitor and correct for anomalous fading (cf., Lowick et al., 2012), the IRSL ages should also be interpreted as minimum ages. While we cannot resolve our age discrepancies, these observations are of concern for previous and future studies employing luminescence dating on fill terraces in the Himalaya, where poor sensitivity and low brightness is a common problem (Owen et al., 2008).

Making matters worse, the  $^{14}\text{C}$  ages of samples DS6-013 and -014 are inverted with respect to the stratigraphic order. Although isolated remnants of an older valley fill suggest that erosive contacts with the younger valley fill exist, we took these samples from an extensive and well accessible outcrop (Fig. 3, Fig. S8) and deem the chance to have misinterpreted the sampled stratigraphy low. Moreover, a misinterpreted stratigraphy would not explain the mismatch of ages derived from the same deposits but different dating methods. Instead, we cannot exclude that some of the organic material consists of older, reworked detrital material that may have been temporarily stored in colluvial hollows. Although this seems reasonable, it cannot be further tested. Because a significant source of non-organic, dead carbon in the sample material can be excluded, at the very least, our  $^{14}\text{C}$  dates provide us with maximum depositional ages.

In summary, although our geochronology samples do not allow us to constrain the timing of the aggradation period as precisely as we would have wished for, they provide us with first-order

constraints that are pertinent to interpreting the geomorphic history and our paleo-erosion rate samples. First, the minimum depositional ages provided by the OSL and IRSL data indicate that aggradation of the valley fill occurred during the late Pleistocene, probably after 50 ka, as constrained by the oldest  $^{14}\text{C}$  age. Termination of the aggradation period and onset of incision by  $\sim 10\text{--}15$  ka is indicated by our  $^{10}\text{Be}$  surface-exposure ages from terraces in the Tons and Yamuna valleys, which are in agreement with a 9.9 ka exposure age for the topmost terrace surface of a similar valley fill in the nearby Sutlej Valley (Bookhagen et al., 2006). In this context it is important to note that the incision of fans and terraces in the nearby Bhagirathi Valley (Fig. 2), which are related to glacial and paraglacial sedimentation, occurred mostly during the Holocene (Barnard et al., 2004). These data therefore support a model of river aggradation that occurred during the more arid late Pleistocene, and an incision of the valley fill during the more humid Holocene (e.g., Srivastava et al., 2008). Previously published luminescence ages from the NW Himalaya could be similar problematic as our samples, and should therefore be interpreted as minimum ages, too. However, even with this caveat in mind, all available minimum ages from terraces and alluvial fans support that aggradation occurred regionally and during the Pleistocene (Fig. 6), thus reinforcing a climatic cause. We also note that the restricted upstream extent of terraces in the Tons Valley is compatible with previously reconstructed glacial extents (Scherler et al., 2010) and with aggradation that was contemporaneous with more extensive glaciers during the late Pleistocene. Second, based on the  $^{10}\text{Be}$  half-life of  $\sim 1.4$  Myr, depositional ages of up to 50 ka would result in maximum losses of  $\sim 2.5\%$  of the initial nuclides by radioactive decay. Because this fraction is small compared to other uncertainties, we neglect radioactive decay after deposition and directly compare recent and paleo-erosion rates.

### 6.2. Temporal variations in erosion rates

Compared to the previously published  $^{10}\text{Be}$  concentrations of modern river sediments with identical upstream areas (Scherler et al., 2014a), six out of seven terrace samples have lower concentrations (Fig. 7a). Before we can assign these differences to true temporal variations in erosion rate, we need to discuss some complicating factors that probably bias our estimates. First, it is likely that the modern samples contain some terrace material and therefore reflect a mixed signal of recent and paleo-erosion rates. We used the estimated trunk valley fill volumes and modern erosion rates to assess the potential magnitude of mixing (Table EA5). For an onset and steady incision of the valley fill since  $\sim 10$  ka, the average contribution of valley fill material to the modern sediments lies between  $<5\%$  for the upstream sites (P1, T1, Y1) and up to  $\sim 40\%$  for the downstream sites (T2, Y2), considering only the valley fill from the trunk valleys. Because average terrace incision rates were in most places rapid ( $10\text{--}15 \text{ mm yr}^{-1}$  for an onset of incision at 10 ka), the bulk of the terrace sediments would have come from well-shielded depths within the valley fill, leading to dilution of the modern river sands with material of lower  $^{10}\text{Be}$  concentration. Thus, the modern  $^{10}\text{Be}$  concentrations acquired on hillslopes would have to be even higher than suggested by the measured concentrations, resulting in lower recent erosion rates and a greater difference with the paleo-erosion rates.

Second, it is likely that the terrace sediments continued accumulating  $^{10}\text{Be}$  after their deposition. If we assume that deposition of the currently exposed valley fill occurred steadily between 40 ka (20 ka) and 10 ka, the resulting aggradation rates at the sites of our samples range between  $\sim 1.8$  and  $4.6 \text{ mm yr}^{-1}$  (5.5 and  $13.9 \text{ mm yr}^{-1}$ ); the lower rates being associated with the shallow valley-fill exposure in the Pabbar Valley (P1). The relative contribution of  $^{10}\text{Be}$  to our samples after deposition and before incision of

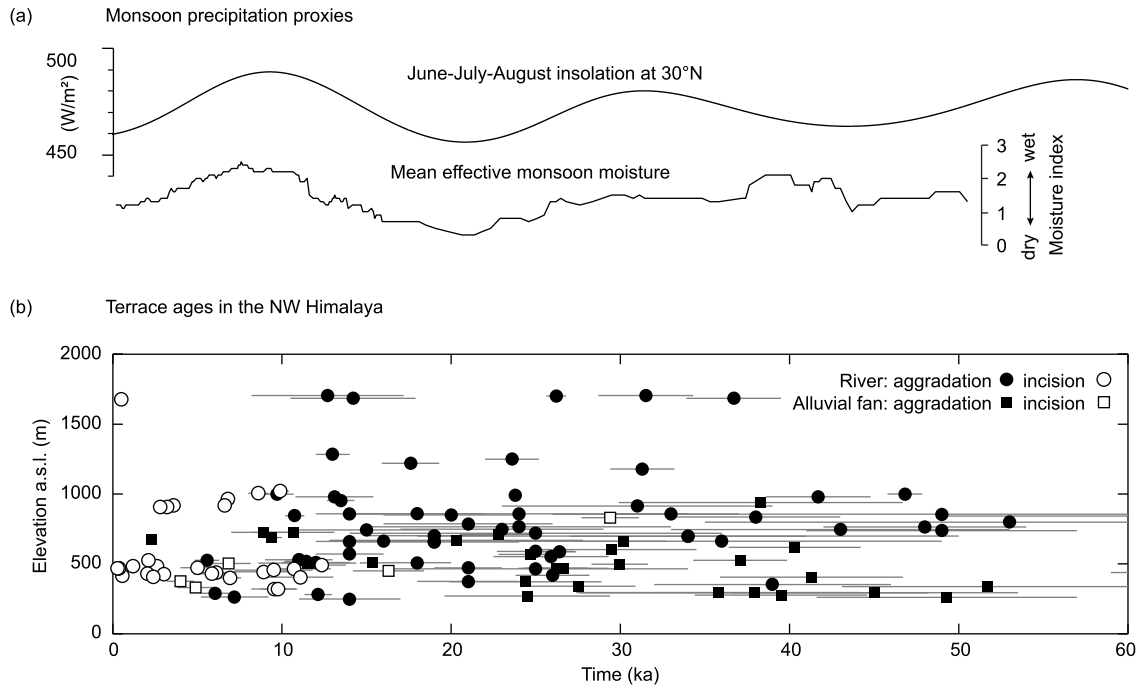


**Fig. 6.** Monsoonal variation and geomorphic events in the NW Himalaya. (a) Indian monsoon strength proxies. Average June–July–August insolation at 30°N after Huybers (2006), and mean effective monsoon moisture from stacked lake records after Herzschuh (2006). (b) Compilation of terrace ages from the NW Himalaya (Singh et al., 2001; Bookhagen et al., 2005; Suresh et al., 2007; Srivastava et al., 2008; Sinha et al., 2010; Ray and Srivastava, 2010; Dutta et al., 2012; this study). Black data points indicate samples from the interior of terraces. White data points indicate samples from floodplain sediments on cut terraces.

**Table 3**  
<sup>10</sup>Be-derived erosion rates.

Locality	Late Pleistocene erosion rate, depending on depositional age ( $t_d$ ), and snowline lowering ( $\Delta SL$ ) <sup>a</sup>						Recent erosion rate <sup>b</sup> [ $t = 0$ ka]
	[ $t_d = 0$ ka]	[ $t_d = 10$ ka]	[ $t_d = 20$ ka]	[ $t_d = 20$ ka, $\Delta SL = 500$ m]	[ $t_d = 20$ ka, $\Delta SL = 1000$ m]	[ $t_d = 40$ ka]	
P1	1.25 ± 0.10	1.31 ± 0.10	1.46 ± 0.12	1.32 ± 0.10	1.21 ± 0.09	1.73 ± 0.14	0.35 ± 0.03
T1	2.14 ± 0.18	2.23 ± 0.18	2.47 ± 0.21	2.28 ± 0.19	2.14 ± 0.18	2.93 ± 0.25	1.22 ± 0.10
T2	0.69 ± 0.05	0.72 ± 0.06	0.80 ± 0.06	0.75 ± 0.06	0.71 ± 0.05	0.93 ± 0.07	1.13 ± 0.09
Y1	1.36 ± 0.11	1.42 ± 0.11	1.58 ± 0.12	1.48 ± 0.12	1.37 ± 0.11	1.87 ± 0.15	1.14 ± 0.09
Y2	1.06 ± 0.08	1.10 ± 0.09	1.22 ± 0.10	1.17 ± 0.09	1.11 ± 0.09	1.43 ± 0.12	0.31 ± 0.02
Y2	1.50 ± 0.11	1.56 ± 0.12	1.73 ± 0.13	1.66 ± 0.13	1.56 ± 0.12	2.03 ± 0.16	0.31 ± 0.02
Y2	0.59 ± 0.04	0.61 ± 0.05	0.68 ± 0.05	0.65 ± 0.05	0.62 ± 0.05	0.79 ± 0.06	0.31 ± 0.02

<sup>a</sup> All erosion rates based on a time-dependent version of the production-rate scaling scheme after Lal (1991) and Stone (2000), denoted 'Lm' in Balco et al. (2008).

<sup>b</sup> Recent erosion rates from Scherler et al. (2014a).

the valley fill would have been ∼5–33% (2–16%) of the measured concentrations (Table EA6). Again, subtracting these contributions would further augment the differences in erosion rates that we observe. We note that some of the highest relative contributions are expected for sample locations T1 and Y1 (Table EA6), where the ratio between late Pleistocene and recent erosion rates is among the lowest.

Third, shielding by snow and ice coverage was likely higher during glacial periods. Our approach to address changes in snow-cover shielding has shown that reductions of paleo-erosion rates by up to ∼15% are conceivable for some samples. On the other hand, if concurrently with snowlines, treelines were also lowered, the change in tree cover would most likely have reduced the shielding through vegetation, at least for elevations near the present-day treeline. The largest effect of changes in ice-cover shielding is expected for the upper Tons Valley, where late Pleistocene ice cover was at least ∼163 km<sup>2</sup>, compared to presently ∼98 km<sup>2</sup> (Scherler et al., 2010). For our highest sample in the Tons Valley (DS7-80, upstream area ∼3400 km<sup>2</sup>) this is less than 5% of the upstream area. Acknowledging more extensive ice coverage in the adjoining tributaries of the upper Tons Valley, this number could easily double. Because ice coverage would preferentially shield sites of high production rate, it is possible that the paleo-erosion rates from the Tons Valley

are biased towards higher rates. In the Yamuna and Pabbar valleys, however, where evidence for ice coverage is limited, the impact of changes in ice cover on catchment-average production rates was most likely small.

In summary, most of our samples are affected by a number of corrections, which are difficult to constrain precisely. However, the above discussion has shown that corrections due to recycling of terrace sediments and post-depositional <sup>10</sup>Be production would augment the differences between recent and paleo-erosion rates that we observe. Furthermore, if the lower <sup>10</sup>Be concentrations in the terrace sediments were largely due to the contribution of shielded subglacial sediments, we would expect this effect to be more pronounced in the Tons compared to the Yamuna and Pabbar valleys, which is not the case. We therefore suggest that our samples record a true decrease in erosion rates between the late Pleistocene and the present-day. Because we were not able to precisely constrain the depositional ages of our terrace samples, we cannot give definitive paleo-erosion rate estimates (Table 3). However, for depositional ages between 10 and 40 ka, the average paleo-erosion rate is higher by a factor of ∼2, but with large variations between the samples (Fig. 7a). When taking the relative position within the valley fill as a measure of time and assuming simultaneous deposi-

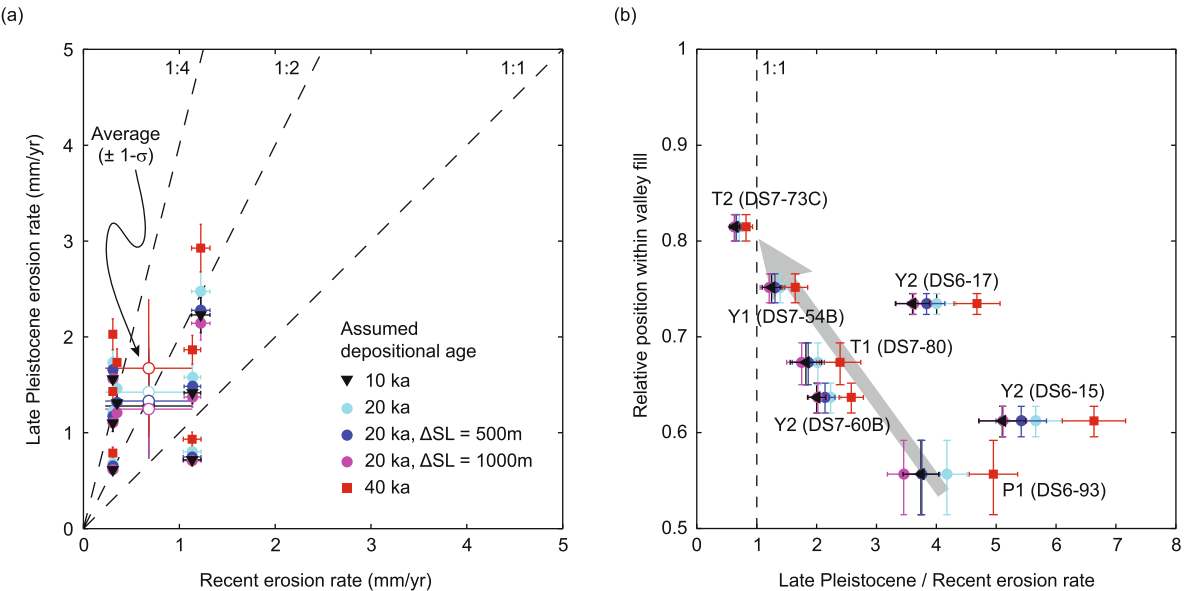


**Fig. 7.** (a)  $^{10}\text{Be}$ -derived recent erosion rates from river sediments versus late Pleistocene erosion rates from terrace sediments. Colors and symbols denote different assumed depositional ages and changes in snowline elevation ( $\Delta\text{SL}$ ). (b) Ratio of recent and late Pleistocene erosion rates versus relative position within the valley fill, as measured from the estimated bedrock contact. Y-axis error bar is based on  $\pm 10$  m uncertainty in estimated bedrock elevation. See text for details. (For interpretation of the references to color in this figure legend, the reader is referred to the web version of this article.)

tion throughout the study area, we observe that erosion rates were apparently decreasing during the course of aggradation (Fig. 7b).

### 6.3. Response of hillslopes and rivers to late Pleistocene climate change

In the model of hillslope-driven aggradation, hillslope-erosion rates peaked during the early Holocene due to enhanced precipitation and landsliding (Pratt et al., 2002; Bookhagen et al., 2005). Similarly, it has been suggested that changes towards a wetter climate would force hillslopes in the Himalaya to lower their angles by deep-seated bedrock landslides and thereby increase hillslope erosion rates (Gabet et al., 2004). In contrast, our results suggest that erosion rates in the Garhwal Himalaya were higher during the late Pleistocene compared to the present day (Fig. 7a). Although we could not directly quantify erosion rates during the early Holocene, both the timing of incision and the apparent decrease of erosion rates during valley aggradation are inconsistent with hillslope-driven aggradation during the early Holocene, which would require erosion rates to progressively increase as hillslope sediments are depleting (Fig. 1c).

Because higher late Pleistocene erosion rates in the Yamuna and Pabbar valleys are difficult to explain by glacial erosion, other processes must be invoked. Relative to physical erosion, chemical weathering is small in the Garhwal Himalaya (Dalai et al., 2002) and changes therein are unlikely to affect total erosion rates by much. Alternatively, the physical disintegration of bedrock by the action of frost is well known to be temperature sensitive (e.g., Walder and Hallet, 1985) and capable of producing large volumes of debris, particularly in steep mountainous regions, if moisture supply is sufficient (Hales and Roering, 2005), which is certainly the case in the monsoonal Himalaya. For example, cooler temperatures during glacial times would shift the loci of rock fracture by frost to lower elevations (Scherler, 2014), which would increase the areal extent of periglacial sediment production and might account for higher late Pleistocene erosion rates. In this case, gradual warming towards the end of the late Pleistocene could be an explanation for the apparent decrease of erosion rates during the aggradation period; a hypothesis that could be tested with better chronological control. If it were true, reduced discharge and

enhanced hillslope sediment supply could have been equally important for driving the aggradation.

We argue, however, that in rapidly eroding landscapes, where hillslopes are at their critical angle of stability and where most mass wasting occurs by landslides (e.g., Burbank et al., 1996), hillslope erosion rates that decrease during aggradation periods should be expected, even under constant climate. As rivers aggrade and valley bottoms rise, hillslopes will gradually attain less steep angles, due to reduced undercutting and oversteepening, and hence landslides are less frequently triggered. The resulting increase in hillslope-sediment residence times lowers hillslope erosion rates. Therefore, if the principal cause for river aggradation was a reduction in stream capacity (discharge-driven aggradation) due to reduced or less flashy discharge, for example, the decreasing supply of sediments from hillslopes would have been the consequence. In this case, the similarity of erosion rates at the end of the aggradation period and during the present-day (Fig. 7b) could be interpreted to indicate that hillslopes are still accumulating sediments where they are buffered by river terraces in their lower parts, or where the rivers have not yet reached bedrock again. Although this can be excluded for bedrock hillslopes in large parts of the High Himalaya, where no valley fill was ever deposited (Fig. 4), it may be an important but so far neglected factor for soil-mantled and vegetated hillslopes in the more slowly eroding Lesser Himalaya. If true, it would imply that erosion rates based on  $^{10}\text{Be}$  concentrations in modern stream sediments underestimate long-term erosion rates in the Lesser Himalaya.

## 7. Conclusions

Our study has shown that widespread fluvial aggradation in the NW Himalaya occurred during the late Pleistocene and terminated at the onset of the Holocene. Minor glacial influence in the Yamuna and Pabbar catchments shows that glaciation in the headwaters is no prerequisite for valley-floor aggradation. Comparison of  $^{10}\text{Be}$  concentrations in stream and terrace sediments from the Yamuna catchment indicates that late Pleistocene erosion rates were higher than recent erosion rates by a factor of  $\sim 2\text{--}4$ . These findings suggest that aggradation in the Yamuna catchment likely resulted from a combination of reduced discharge and in-

creased sediment supply during the late Pleistocene and not, as previously suggested for other Himalayan catchments, by the impulsive release of hillslope sediments during the early Holocene, when monsoon precipitation was more intense. Our data furthermore indicate that erosion rates decreased during the time of aggradation, which could be related to either a temperature control on sediment production, e.g., through periglacial weathering, but is also consistent with threshold hillslopes that were relaxing when river incision stopped and local base levels were rising. Until today, an estimated ~80% of the sediments stored in the three main valleys of the Yamuna catchment have been eroded, and likely more in the tributaries. Where rivers have not yet reached bedrock again, hillslopes might still retain material that accumulated during aggradation and incision of the valley fill, with the consequence that present-day  $^{10}\text{Be}$ -derived hillslope erosion rates may not be in equilibrium with long-term incision rates.

## Acknowledgements

This research was funded by the DFG graduate school GK1364 (DFG grant STR373/21-1). D.S. is grateful for support by the Alexander von Humboldt Foundation through a Feodor Lynen Research Fellowship and for discussions with J.-P. Avouac, M. Lamb, and T. Schildgen. We thank T. Tsering Lonpo for support during fieldwork. We appreciate the thorough and constructive reviews by three anonymous reviewers.

## Appendix A. Supplementary material

Supplementary material related to this article can be found online at <http://dx.doi.org/10.1016/j.epsl.2015.06.034>. These data include the Google map of the most important areas described in this article.

## References

- Arendt, A., et al., 2012. Randolph Glacier Inventory [v2.0]: A Dataset of Global Glacier Outlines. Global Land Ice Measurements from Space. Boulder Colorado, USA: Digital Media.
- Balco, G., Stone, J., Lifton, N., Dunai, T., 2008. A complete and easily accessible means of calculating surface exposure ages or erosion rates from  $^{10}\text{Be}$  and  $^{26}\text{Al}$  measurements. *Quat. Geochronol.* 3, 174–195. <http://dx.doi.org/10.1016/j.quageo.2007.12.001>.
- Barnard, P.L., Owen, L.A., Finkel, R.C., 2004. Style and timing of glacial and paraglacial sedimentation in a monsoonal influenced high Himalayan environment, the upper Bhagirathi Valley, Garhwal Himalaya. *Sediment. Geol.* 165, 199–221.
- Bekaddour, T., et al., 2014. Paleo erosion rates and climate shifts recorded by Quaternary cut-and-fill sequences in the Pisco valley, central Peru. *Earth Planet. Sci. Lett.* 390, 103–115.
- Bookhagen, B., Burbank, D.W., 2010. Toward a complete Himalayan hydrological budget: spatiotemporal distribution of snowmelt and rainfall and their impact on river discharge. *J. Geophys. Res.* 115, F03019. <http://dx.doi.org/10.1029/2009jf001426>.
- Bookhagen, B., Fleitmann, D., Nishizumi, K., Strecker, M.R., Thiede, R., 2006. Holocene monsoonal dynamics and fluvial terrace formation in the northwest Himalaya, India. *Geology* 34 (7), 601–604. <http://dx.doi.org/10.1130/G22698.1>.
- Bookhagen, B., Thiede, R.C., Strecker, M.R., 2005. Late Quaternary intensified monsoon phases control landscape evolution in the northwest Himalaya. *Geology* 33, 149–152.
- Bull, W.B., 1991. *Geomorphic Response to Climate Change*. Oxford University Press, New York.
- Burbank, D.W., Leland, J., Fielding, E., Anderson, R.S., Brozović, N., Reid, M.R., Duncan, C., 1996. Bedrock incision, rock uplift and threshold hillslopes in the northwestern Himalayas. *Nature* 379, 505–510. <http://dx.doi.org/10.1038/379505a0>.
- Carson, M.A., 1976. Mass-wasting, slope development and climate. In: Derbyshire, E. (Ed.), *Geomorphology and Climate*. John Wiley and Sons, New York, pp. 101–136.
- Charreau, J., Plard, P.-H., Puchol, N., Avouac, J.-P., Lallier-Vergès, E., Bourlès, D., Braucher, R., Gallaud, A., Finkel, R., Jolivet, M., Chen, Y., Roy, P., 2011. Paleoenvironmental evidence for a transient increase in monsoon intensity in Central Asia since 9 Ma: implications for Quaternary glaciations? *Earth Planet. Sci. Lett.* 304, 85–92.
- Clemens, S., Prell, W., Murray, D., Shimmield, G., Weedon, G., 1991. Forcing mechanisms of the Indian Ocean monsoon. *Nature* 353, 720–725.
- Dalai, T.K., Krishnaswami, S., Sarin, M.M., 2002. Major ion chemistry in the headwaters of the Yamuna River System: chemical weathering, its temperature dependence and  $\text{CO}_2$  consumption in the Himalaya. *Geochim. Cosmochim. Acta* 66, 3397–3416.
- Dutta, S., Suresh, N., Kumar, R., 2012. Climatically controlled Late Quaternary terrace staircase development in the fold-and-thrust belt of the Sub Himalaya. *Paleogeogr. Palaeocl.* 356–357, 16–26.
- Gabet, E., Burbank, D.W., Putkonen, J.K., Pratt-Sitaula, B.A., Ojha, T., 2004. Rainfall thresholds for landsliding in the Himalayas of Nepal. *Geomorphology* 63, 131–143. <http://dx.doi.org/10.1016/j.geomorph.2004.03.011>.
- Gansser, A., 1964. *Geology of the Himalayas*. Interscience, London.
- Granger, D.E., Kirchner, J.W., Finkel, R., 1996. Spatially averaged long-term erosion rates from in-situ produced cosmogenic nuclides in alluvial sediment. *J. Geol.* 104, 249–257.
- Hales, T.C., Roering, J.J., 2005. Climate-controlled variations in scree production, Southern Alps, New Zealand. *Geology* 33, 701–704. <http://dx.doi.org/10.1130/G21528.1>.
- Herzschuh, U., 2006. Paleo-moisture evolution in monsoonal Central Asia during the last 50,000 years. *Quat. Sci. Rev.* 25, 163–178.
- Huybers, P., 2006. Early Pleistocene glacial cycles and the integrated summer insolation forcing. *Science* 313, 508–511.
- Juyal, N., Sundriyal, Y., Rana, N., Chaudhary, S., Singhvi, A.K., 2010. Late Quaternary fluvial aggradation and incision in the monsoon-dominated Alaknanda valley, Central Himalaya, Uttrakhand, India. *J. Quat. Sci.* 25 (8), 1293–1304.
- Lal, D., 1991. Cosmic-ray labeling of erosion surfaces: in situ nuclide production rates and erosion models. *Earth Planet. Sci. Lett.* 104 (2–4), 424–439.
- Lavé, J., Avouac, J.-P., 2001. Fluvial incision and tectonic uplift across the Himalayas of central Nepal. *J. Geophys. Res.* 106, 26561–26591.
- Lowick, S.E., Trauerstein, M., Preusser, F., 2012. Testing the application of post IR-IRSL dating to fine grain waterlain sediments. *Quat. Geochronol.* 8, 33–40.
- Lupker, M., Blard, P.-H., Lavé, J., France-Lanord, C., Leanni, L., Puchol, N., Charreau, J., Bourlès, D., 2012.  $^{10}\text{Be}$ -derived Himalayan denudation rates and sediment budgets in the Ganga basin. *Earth Planet. Sci. Lett.* 333–334, 146–156. <http://dx.doi.org/10.1016/j.epsl.2012.04.020>.
- Murray, A.S., Wintle, A.G., 2000. Luminescence dating of quartz using an improved single-aliquot regenerative-dose protocol. *Radiat. Meas.* 32, 57–73.
- Owen, L.A., Caffee, M.W., Finkel, R.C., Seong, Y.B., 2008. Quaternary glaciation of the Himalayan-Tibetan orogeny. *J. Quat. Sci.* 23 (6–7), 513–531.
- Powers, P.M., Lillie, R.J., Yeats, R.S., 1998. Structure and shortening of the Kangra and Dehra Dun reentrants, Sub-Himalaya, India. *Geol. Soc. Am. Bull.* 110, 1010–1027. [http://dx.doi.org/10.1130/0016-7606\(1998\)110<1010:SASOUD>2.3.CO;2](http://dx.doi.org/10.1130/0016-7606(1998)110<1010:SASOUD>2.3.CO;2).
- Pratt, B., Burbank, D.W., Heimsath, A., Ojha, T., 2002. Impulsive alluviation during early Holocene strengthened monsoons, central Nepal Himalaya. *Geology* 30, 911–914. [http://dx.doi.org/10.1130/0091-7613\(2002\)030<911:IATHD>2.3.CO;2](http://dx.doi.org/10.1130/0091-7613(2002)030<911:IATHD>2.3.CO;2).
- Pratt-Sitaula, B., Garde, M., Burbank, D.W., Osokin, M., Heimsath, A., Gabet, E., 2007. Bedload-to-suspended load ratio and rapid bedrock incision from Himalayan landslide-dam lake record. *Quat. Res.* 68, 111–120.
- Ray, Y., Srivastava, P., 2010. Widespread aggradation in the mountainous catchment of the Alaknanda-Ganga River System: timescales and implications to Hinterland-foreland relationships. *Quat. Sci. Rev.* 29, 2238–2260.
- Reimer, P.J., et al., 2013. IntCal13 and Marine13 radiocarbon age calibration curves, 0–50,000 years calBP. *Radiocarbon* 55 (4). [http://dx.doi.org/10.2458/azu\\_js\\_rc.55.16947](http://dx.doi.org/10.2458/azu_js_rc.55.16947).
- Riebe, C.S., Kirchner, J.W., Granger, D.E., Finkel, R.C., 2001. Minimal climatic control on erosion rates in the Sierra Nevada. *Geology* 29 (5), 447–450.
- Schaller, M., Ehlers, T., 2006. Limits to quantifying climate driven changes in denudation rates with cosmogenic nuclides. *Earth Planet. Sci. Lett.* 248, 153–167.
- Schaller, M., von Blanckenburg, F., Veldkamp, A., Tebbens, L.A., Hovius, N., Kubik, P.W., 2002. A 30 000 yr record of erosion rates from cosmogenic  $^{10}\text{Be}$  in Middle European river terraces. *Earth Planet. Sci. Lett.* 204, 307–320.
- Scherler, D., 2014. Climatic limits to headwall retreat in the Khumbu Himalaya, eastern Nepal. *Geology* 42, 1019–1022. <http://dx.doi.org/10.1130/G35975.1>.
- Scherler, D., Bookhagen, B., Strecker, M.R., 2014a. Tectonic control on  $^{10}\text{Be}$ -derived erosion rates in the Garhwal Himalaya, India. *J. Geophys. Res.* 118, 1–24. <http://dx.doi.org/10.1002/2013jf002955>.
- Scherler, D., Munack, H., Mey, J., Eugster, P., Wittmann, H., Codilean, A.T., Kubik, P., Strecker, M.R., 2014b. Ice dams, outburst floods, and glacial incision at the western margin of the Tibetan Plateau: A > 100 k.y. chronology from the Shyok Valley, Karakoram. *Geol. Soc. Am. Bull.* 126, 738–758. <http://dx.doi.org/10.1130/B30942.1>.
- Scherler, D., Bookhagen, B., Strecker, M.R., von Blanckenburg, F., Rood, D., 2010. Timing and extent of late Quaternary glaciation in the western Himalaya constrained by  $^{10}\text{Be}$  moraine dating in Garhwal, India. *Quat. Sci. Rev.* 29, 815–831.
- Schwanghart, W., Scherler, D., 2014. Short Communication: TopoToolbox 2 – MATLAB-based software for topographic analysis and modeling in Earth surface sciences. *Earth Surf. Dyn.* 2, 1–7. <http://dx.doi.org/10.5194/esurf-2-1-2014>.
- Singh, A.K., Parkash, B., Mohindra, R., Thomas, J.V., Singhvi, A.K., 2001. Quaternary alluvial fan sedimentation in the Dehradun Valley Piggyback Basin, NW Himalaya: tectonic and paleoclimatic implications. *Basin Res.* 13, 449–471.

- Sinha, S., Suresh, N., Kumar, R., Dutta, S., Arora, B.R., 2010. Sedimentologic and geomorphic studies on the Quaternary alluvial fan and terrace deposits along the Ganga exit. *Quat. Int.* 227, 87–103.
- Srivastava, P., Tripathi, J.K., Islam, R., Jaiswal, M.K., 2008. Fashion and phases of late Pleistocene aggradation and incision in the Alaknanda River Valley, western Himalaya, India. *Quat. Res.* 70, 68–80.
- Staiger, J., Gosse, J., Toracinta, R., Oglesby, B., Fastook, J., Johnson, J.V., 2007. Atmospheric scaling of cosmogenic nuclide production: climate effect. *J. Geophys. Res.* 112, B02205. <http://dx.doi.org/10.1029/2005JB003811>.
- Steffen, D., Schlunegger, F., Preusser, F., 2009a. Drainage basin response to climate change in the Pisco valley, Peru. *Geology* 37, 491–494.
- Steffen, D., Preusser, F., Schlunegger, F., 2009b. OSL quartz age underestimation due to unstable signal components. *Quat. Geochronol.* 4, 353–362.
- Stone, J.O., 2000. Air pressure and cosmogenic isotope production. *J. Geophys. Res.* 105, 23,753–23,759.
- Suresh, N., Bagati, T.N., Kumar, R., Thakur, V.C., 2007. Evolution of Quaternary alluvial fans and terraces in the intramontane Pinjaur Dun, Sub-Himalaya, NW India: interaction between tectonics and climate change. *Sedimentology* 54, 809–833.
- Tucker, G.E., Slingerland, R., 1997. Drainage basin responses to climate change. *Water Resour. Res.* 33, 2031–2047.
- von Blanckenburg, F., 2005. The control mechanisms of erosion and weathering at basin scale from cosmogenic nuclides in river sediment. *Earth Planet. Sci. Lett.* 237, 462–479.
- Walder, J., Hallet, B., 1985. A theoretical model of the fracture of rock during freezing. *Geol. Soc. Am. Bull.* 96, 336–346. [http://dx.doi.org/10.1130/0016-7606\(1985\)96<336:ATMOT>2.0.CO;2](http://dx.doi.org/10.1130/0016-7606(1985)96<336:ATMOT>2.0.CO;2).
- Wulf, H., Bookhagen, B., Scherler, D., 2010. Seasonal precipitation gradients and their impact on fluvial sediment flux in the northwest Himalaya. *Geomorphology* 118 (1–2), 13–21. <http://dx.doi.org/10.1016/j.geomorph.2009.12.003>.